Journal of Power Sources 209 (2012) 282–288

Contents lists available at SciVerse ScienceDirect

Journal of Power Sources

journal homepage: www.elsevier.com/locate/jpowsour

Controls oriented reduced order modeling of solid-electrolyte interphase layer growth

Alfred V. Randall[a], Roger D. Perkins[a], Xiangchun Zhang[b], Gregory L. Plett[a,*]

[a] Department of Electrical and Computer Engineering, University of Colorado Colorado Springs, Colorado Springs, CO 80918, United States
[b] Sakti3, 1490 Eisenhower Place, Building 4, Ann Arbor, MI 48108-3283, United States

ARTICLE INFO

Article history:
Received 2 January 2012
Received in revised form 28 February 2012
Accepted 29 February 2012
Available online 7 March 2012

Keywords:
Solid electrolyte interphase
Lithium ion cell degradation
Incremental reduced order model

ABSTRACT

Battery cell life depends critically on how the cell is used. Therefore, battery chargers and battery management systems must be designed to control cell usage carefully. In order to design optimal battery controls that effect a tradeoff between cell performance (in some sense) and cell life, a model of cell degradation is necessary. This model must be simple and incremental in order to be implemented by an inexpensive microcontroller. This paper takes a first step toward developing such a controls-oriented comprehensive cell degradation model by deriving a reduced-order model of a single mechanism: the growth process of the solid-electrolyte interphase (SEI) layer, along with the resulting resistance rise and capacity loss. This reduced-order model approximates a physics-based PDE model from the literature, is simple and accurate, and may be used in optimal strategies for controlling lithium-ion batteries.

1. Introduction

Many applications of battery packs require high power and long life. These two objectives are at odds with each other since, in general, high charge and discharge rates accelerate aging. It is our ultimate goal to design methods to control a battery pack to effect an optimum tradeoff between performance and degradation, and to do so we will need mathematical models of the dominant cell degradation mechanisms. These models must be simple enough to be quickly executed on an inexpensive embedded systems processor.

Presently, many battery management systems (BMS) track macroscopic indicators of aging such as capacity fade and power fade but few, if any, track physical indicators of aging such as degree of solid-electrolyte-interphase (SEI) layer growth on anode particles, degree of lithium plating on anode particles, degree of cathode dissolution, and so forth. However, identical combinations of capacity loss and resistance rise might be achieved by traveling different paths—by exciting different physical mechanisms of degradation—yielding potentially different resultant optimal control strategies for operating the battery pack. Therefore, knowing cell resistance and capacity alone is not sufficient to extend cell life to the maximum extent via control.

We believe that by modeling the dominant physical degradation mechanisms that occur in a cell, and then by using those models in an optimized predictive control algorithm, battery life can be extended. For a practical implementation, this requires that the degradation model be *simple* and *incremental*. We consider a model to be simple if it is described by a small number of ordinary difference equations, and incremental (or recursive) if it predicts a future degradation state based on a present degradation state and a proposed cell input current. The model will necessarily be a function of cell temperature, state-of-charge (SOC), and possibly other factors as well.

Degradation leading to capacity loss and resistance rise can occur either due to mechanical stress factors or chemical side reactions [1–8]. Various schemes have been introduced to model side reactions, including that of Darling and Newman, who first introduced the concept of modeling parasitic effects in lithium-ion batteries by modeling solvent oxidation side reactions [3]. More recently, Ramadass and colleagues have proposed a model that describes the formation and growth of an SEI layer on anode solid particles during charging, that uses solvent reduction as the main side reaction mechanism for degradation [9]. The present paper builds on and extends this work to propose a simple incremental model of SEI growth and associated capacity loss and resistance rise. The proposed model may then be used in an optimal control scheme that will reduce side reactions and limit cell degradation. (The control task is the subject of present research, and will be reported in a later paper. The methodology presented in [10] is one possible approach.) While various efforts have been made to create reduced-order models of ideal-cell dynamics (*i.e.*, models that do not consider degradation), including single particle models by

* Corresponding author. Tel.: +1 719 255 3468; fax: +1 719 255 3589.
E-mail addresses: alfred.randall@colorado.edu (A.V. Randall), rperkin3@uccs.edu (R.D. Perkins), xcz@sakti3.com (X. Zhang), gplett@uccs.edu (G.L. Plett).

0378-7753/$ – see front matter © 2012 Elsevier B.V. All rights reserved.
doi:10.1016/j.jpowsour.2012.02.114

Nomenclature

a	specific surface area of porous electrode, m^{-1}
brug	Bruggeman exponent, unitless
c	concentration of Li or Li^+ ions, mol m^{-3}
D	diffusion coefficient, m^2 s^{-1}
F	Faraday's constant, 96 487 C mol^{-1}
i_0	exchange-current density for intercalation reaction, A m^{-2}
$i_{0,s}$	exchange-current density for side reaction, A m^{-2}
J_I	local volumetric current density for intercalation reaction, A m^{-3}
J_s	local volumetric current density for side reaction, A m^{-3}
k	rate constant of electrochemical reaction, A $m^{5/2}$ $mol^{-3/2}$
L	length of cell, m
Q	cell capacity, C
R	particle radius, μm
R_{film}	film resistance at the electrode/electrolyte interface, Ω m^2
R_g	universal gas constant, 8.314 J mol^{-1} K^{-1}
T	temperature, K
t	time, s
t_+^0	transport number, unitless
U	local equilibrium potential, V
x	length dimension, m

Greek

α_a, α_c	anodic and cathodic transfer coefficients of electrochemical reaction, unitless
ε	volume fraction of a phase, unitless
ϕ	local potential of a phase, V
η	local overpotential driving electrochemical reaction, V
κ	conductivity of electrolyte, S m^{-1}
θ	state-of-charge or stoichiometry of electrode
σ	conductivity of electrode, S m^{-1}
ρ	density of active material, kg m^{-3}
δ	film thickness, m

Subscript/superscript

e	pertaining to the electrolyte phase
s	pertaining to the solid phase
n	pertaining to the negative electrode
p	pertaining to the positive electrode

Chaturvedi et al. [11] and one-dimensional models by Smith et al. [12], we believe this to be the first attempt to create a reduced-order model to describe a side reaction.

We note that the field of creating mathematical models of cell degradation mechanisms is still developing. The accuracy of the reduced-order model will be no better than the accuracy of the underlying partial-differential-equation (PDE) model from which it was created. So, it is important for the reader to understand that the purpose of this paper is to propose a methodology for reducing the order of a PDE model of a degradation mechanism to be able to approximate the PDE model with one that can be implemented on a simple microprocessor, such as in one found in a battery management system. For purpose of illustration, we apply the methodology to the specific cell degradation mechanism of SEI layer growth as modeled by Ramadass et al. [9]. The methodology could also be applied to other similar models; for example, as newer and more accurate models are reported in the literature.

In particular, our order-reduction method uses volume averaging to create an algebraic "zero-dimensional" or "0-D" model of the infinite-order PDE model proposed in [9]. This reduced-order model (ROM) of the SEI growth mechanism is a first step toward creating a complete coupled reduced-order model of all dominant cell degradation mechanisms, which then could be used in an optimal control scheme.

This paper will proceed by reviewing the model of SEI layer growth proposed in [9]. A reduced-order volume-averaged approximate model is then derived. Results of pulsed-current simulations of the full-order model and the 0-D reduced-order model are presented and compared, results are discussed, and conclusions are made.

2. Original model

Changes at the electrode/electrolyte interface due to side reactions between the anode and electrolyte are considered to be one of the primary causes of anode aging [8]. There are a large number of reduction reactions that can lead to the deposition of solid products on the anode, and these are less well understood, being very dependent upon the composition of the electrolyte solution [13]. Thus the assumption for the original Ramadass model is that the side reaction is considered to be a consumption of the solvent species and lithium ions, which will form compounds such as Li_2CO_3, LiF, Li_2O, and so forth, depending on the nature of the solvent. Previous studies of the SEI layer formation on lithiated carbon have shown that there is probably significant porosity in the film, and this makes it reasonable to assume that the SEI layer continues to grow as the solvent diffuses through the layer during charge [14–17]. The assumption of the ongoing formation of the SEI layer is also supported by the research of Aurbach and colleagues [14], who propose that the intercalation of lithium into the graphite anode leads to increase in the lattice volume, which in turn stretches the SEI layer, causing it to fracture and to expose more of the anode to the electrolyte, fueling the side reaction, and contributing to SEI formation.

As our goal is to create a high-fidelity reduced-order model of the degradation model in [9], we adopt the same assumptions as they, which were:

1. The main side reaction is due to the reduction of an organic solvent, expressed as $S + 2Li^+ + 2e^- \rightarrow P$, where "S" refers to the solvent and "P" to the product formed in the side reaction.
2. The reaction occurs only during charging of the cell.
3. The products formed are a mixture of different species, resulting in averaged mass and density constants used in the later equation describing the formation and growth of the SEI film.
4. The side reaction is assumed to be irreversible and $U_{ref,s}$ is chosen to be 0.4 V *versus* Li/Li^+.
5. The initial resistance of the SEI layer developed during cell formation is 100 Ω cm^2.
6. There is no overcharge reaction considered (*i.e.*, lithium plating is not modeled).

We have somewhat relaxed Assumption 2, allowing side reactions to occur during rest intervals also (and even during discharge, which we do not report here). The reduced-order modeling method that we present easily incorporates either variant of the assumption.

The SEI growth model of [9] is tightly coupled with a Doyle–Fuller–Newman porous-electrode style model of ideal-cell dynamics [4], which assumes that the solid and electrolyte phases are considered continuous and gives no consideration to the underlying microstructure of the electrode. As porous-electrode theory

is well known, but as there are variants in its implementation, we present those equations in Appendix A, and focus only on the SEI growth model of [9] here.

For the negative electrode the local volumetric transfer current density J_{total} is given by a sum of the intercalation current density J_I and the side reaction current density J_s,

$$J_{\text{total}} = J_I + J_s, \tag{1}$$

where J_I is computed via the Butler–Volmer electrochemical kinetic expression

$$J_I = a_n i_{0,n} \left[\exp\left(\frac{\alpha_{a,n} F}{R_g T} \eta_n \right) - \exp\left(-\frac{\alpha_{c,n} F}{R_g T} \eta_n \right) \right], \tag{2}$$

which is driven by the overpotential

$$\eta_n = \phi_s - \phi_e - U_n^{\text{ref}} - \frac{J_{\text{total}}}{a_n} R_{\text{film}}, \tag{3}$$

where $i_{0,n}$ is the exchange current density and U_n^{ref} is the equilibrium potential which is evaluated as a function of the solid phase concentration at the surface of the particle.

The kinetics of the side reaction are described using a Tafel equation, which assume that the side reaction is considered irreversible,

$$J_s = -i_{0,s} a_n \exp\left(-\frac{\alpha_c F}{R_g T} \eta_s \right) \tag{4}$$

and the side reaction overpotential is described as

$$\eta_s = \phi_s - \phi_e - U_{\text{ref},s} - \frac{J_{\text{total}}}{a_n} R_{\text{film}}. \tag{5}$$

Once the side reaction current, J_s, has been calculated, the change in the film thickness δ_{film} during charging can be calculated by

$$\frac{\partial \delta_{\text{film}}}{\partial t} = -\frac{M_P}{a_n \rho_P F} J_s, \tag{6}$$

where M_P is the average molecular weight of the constituent compounds of the SEI layer and ρ_P is the average density of the constituent compounds. This allows the overall film resistance to be calculated as

$$R_{\text{film}} = R_{\text{SEI}} + \frac{\delta_{\text{film}}}{\kappa_P}, \tag{7}$$

where R_{SEI} is the initial film resistance that is produced during the formation period of the battery, and κ_P is the conductivity of the film.

In addition to the resistance change, there is a capacity loss caused by the side reaction current during charge, leading to capacity changing via the relationship

$$\frac{\partial Q}{\partial t} = \int_0^{L_n} J_s A \, dx. \tag{8}$$

3. Simplifying the model

To effect an optimal control strategy, the processors in battery chargers and battery management systems must be able to calculate the side reaction current density J_s very quickly and accurately. Solving the coupled PDE equations described above is too complicated for such a process. The J_s model needs to be much faster and simpler. In this section, we present a simpler incremental model for calculating J_s, R_{film}, and Q.

To create a volume-averaged 0-D reduced-order model, three additional assumptions are made:

1. The cell is always in a quasi-equilibrium state, allowing the exchange current density $i_{0,n}$ to be calculated from the cell SOC alone, neglecting local variations in electrolyte and solid surface concentration. The estimated value of J_s then corresponds to a suddenly applied current pulse of magnitude i_{app}, which is constant over some time interval Δt.
2. The intercalation current density and the side-reaction current densities are uniform over the anode. This allows us to state that the total reaction current density J_{total} is related to the applied cell current i_{app} by the following relationship:

$$J_{\text{total}} = -\frac{i_{\text{app}}}{\text{Vol}_n}, \tag{9}$$

   where the volume of the active material is described by $\text{Vol}_n = L_n A$.
3. The anodic and cathodic charge-transfer coefficients are equal ($\alpha_a = \alpha_c = 0.5$).

From the above assumptions, an incremental degradation model can be formulated as follows. First, at any point in time, the lithiation state of the anode is calculated as

$$\theta_n = \theta_{n,\min} + \text{SOC}_{\text{cell}} \left(\theta_{n,\max} - \theta_{n,\min} \right), \tag{10}$$

where $\theta_{n,\max}$ and $\theta_{n,\min}$ are the stoichiometric limits of anode lithiation (*i.e.*, the value of θ in $\text{Li}_\theta \text{C}_6$ when the cell is fully charged and discharged, respectively). SOC_{cell} is a value between zero and one, which indicates the cell state-of-charge. Then U_n^{ref} is calculated from θ_n using, for example, Eq. (15).

We will ultimately iterate to find J_s. We can initialize its value to zero and calculate the intercalation current density from Eqs. (1) and (9).

$$J_I = \frac{-i_{\text{app}}}{\text{Vol}_n} - J_s.$$

From J_I and assumption 3, we can manipulate Eq. (2) to find the overpotential for the intercalation reaction to be

$$\eta_n = \frac{2 R_g T}{F} \text{asinh}\left(\frac{J_I}{2 a_n i_0} \right).$$

Then, from Eqs. (3) and (5), the overpotential for the side reaction is:

$$\begin{aligned} \eta_s &= \phi_s - \phi_e - U_{\text{ref},s} - \frac{J_{\text{total}} R_{\text{film}}}{a_n} \\ &= \eta_n + U_n^{\text{ref}} - U_{\text{ref},s}. \end{aligned}$$

We note that the film resistance cancels from the calculation. We can now calculate an updated estimate of the side-reaction current density as

$$J_s = -i_{0,s} a_n \exp\left(\frac{-F}{2 R_g T} \eta_s \right).$$

In total, we have the reduced-order model

$$\begin{aligned} J_s = -i_{0,s} a_n \exp\Bigg(\frac{-F}{2 R_g T} \Bigg(\frac{2 R_g T}{F} \text{asinh}\left(\frac{-i_{\text{app}}/\text{Vol}_n - J_s}{2 a_n i_0} \right) \\ + U_n^{\text{ref}} - U_{\text{ref},s} \Bigg) \Bigg) = -i_{0,s} a_n \exp\left(\frac{-F \left(U_n^{\text{ref}} - U_{\text{ref},s} \right)}{2 R_g T} \right) \\ \times \exp\left(-\text{asinh}\left(\frac{-i_{\text{app}}/\text{Vol}_n - J_s}{2 a_n i_0} \right) \right), \end{aligned}$$

which we iterate until convergence (we find that fewer than ten iterations are generally necessary—the results presented in this paper use exactly ten iterations).

Once we have solved for J_s it can then be incorporated into incremental equations for film resistance and capacity loss. It is assumed

that J_s is constant over some small time interval Δt, and is denoted as $J_s[N]$ for the Nth interval. Since, according to Eq. (6), the change in film thickness is proportional to J_s, we can arrive at an incremental equation for film thickness as

$$\delta_{\text{film}}[N] = \delta_{\text{film}}[N-1] - \frac{M_P \Delta t}{a_n \rho_P F} J_s[N-1],$$

where Δt is the equation update period, and noting that the sign of J_s is negative. This result can be used to calculate the film resistance as

$$R_{\text{film}}[N] = R_{\text{film}}[N-1] - \frac{M_P \Delta t}{a_n \rho_P F \kappa_P} J_s[N-1].$$

Similarly, we can discretize the capacity equation (8) to find that

$$Q[N] = Q[N-1] + (AL_n \Delta t) J_s[N-1].$$

In summary, the proposed reduced-order model (ROM) equations are:

$$\theta_n = \theta_{n,\min} + \text{SOC}_{\text{cell}} \left(\theta_{n,\max} - \theta_{n,\min}\right) \tag{11}$$

$$J_s[N] = -i_{0,s} a_n \exp\left(\frac{-F\left(U_n^{\text{ref}} - U_{\text{ref},s}\right)}{2R_g T}\right) \times \exp\left(-\text{asinh}\left(\frac{-i_{\text{app}}[N]/\text{Vol}_n - J_s[N]}{2a_n i_0}\right)\right) \tag{12}$$

$$R_{\text{film}}[N] = R_{\text{film}}[N-1] - \frac{M_P \Delta t}{a_n \rho_P F \kappa_P} J_s[N-1] \tag{13}$$

$$Q[N] = Q[N-1] + (AL_n \Delta t) J_s[N-1]. \tag{14}$$

4. Comparing the models

The validity of this reduced-order model depends first on the accuracy of the underlying partial differential equation model, which we assume here to be exact. It then depends on how closely the reduced-order approximation of J_s matches the exact calculation of J_s. In this section, results from both the full and reduced-order models for J_s are compared. In addition, the error in J_s is tracked over time in order to see whether the assumption that J_s is constant over a small period of time is reasonable.

To compare the PDE and reduced-order models, we conducted a series of simulations. In each simulation, the cell was initially at rest. A sudden pulse of current was then applied, and the instantaneous resulting J_s from the PDE model was compared to the computed J_s from the ROM. To simulate the PDE model, we used COMSOL Multiphysics 3.5a [18] coupled with a MATLAB [19] script to cycle through the series of simulations and analyze results. Specifically, each simulation comprised a 1 s time interval, where the cell current i_{app} was modeled as a Heaviside step function, which was applied half-way through the interval. We found that the initial rest interval facilitated convergence of the solution by allowing the PDE solver to adjust its initial conditions before applying the step current. (Even so, convergence of the PDE simulations proved troublesome, and required user vigilance to ensure reliable results.) The ROM results were computed by a MATLAB script using Eq. (12).

The cell parameters that we used in the simulations match those used in [9,20] and are listed in Table 1. For the full-order PDE simulations, the applied current was varied between 0 A and 5.4 A (a 3 C rate) in steps of 0.1 A; the initial cell SOC was varied between 0% and 100% in steps of 2%, and temperature was varied between −35 °C and 45 °C in steps of 20 °C. The solver absolute tolerance was set to 10^{-5} and the relative tolerance to 10^{-6}. The default direct UMFPACK solver was used, with 280 mesh points in the 1D battery model and 10 624 elements in the 2D electrode model. The solver timestep was set to 5 ms. A total of 14 025 simulations were run.

Table 1
Electrode parameters for simulation.

Symbol	Units	Anode	Separator	Cathode
L	μm	88	20	80
R	μm	2	–	2
A	m^2	0.0596	0.0596	0.0596
σ	S m^{-1}	100	–	100
ε_s	–	0.49	–	0.59
ε_e	–	0.485	1	0.385
brug	–	4	–	4
$c_s^{\max}$	mol m^{-3}	30 555	–	51 555
c_e^0	mol m^{-3}	1000	1000	1000
$\theta_{i,\min}$	–	0.03	–	0.95
$\theta_{i,\max}$	–	0.886	–	0.487
D_s	$\text{m}^2\ \text{s}^{-1}$	3.9×10^{-14}	–	1.0×10^{-14}
D_e	$\text{m}^2\ \text{s}^{-1}$	7.5×10^{-10}	7.5×10^{-10}	7.5×10^{-10}
t_+^0	–	0.363	0.363	0.363
k	$\text{A m}^{5/2}\ \text{mol}^{-3/2}$	4.854×10^{-6}	–	2.252×10^{-6}
α_a	–	0.5	–	0.5
α_c	–	0.5	–	0.5
$U_{\text{ref},s}$	V	0.4	–	–
$i_{0,s}$	A m^{-2}	1.5×10^{-6}	–	–

For the reduced-order simulations, which run much more quickly, the applied current was varied between 0 A and 5.4 A in steps of 0.05 A; the initial cell SOC was varied between 0% and 100% in steps of 1%, and the temperature was varied between −35 °C and 45 °C in steps of 10 °C. A total of 112 200 simulations were run. As one point of comparison, the set of 14 025 full-order PDE simulations took more than eight days to complete on an Intel i7 processor, while the set of 112 200 ROM simulations took a total of about 2.6 s to complete on the same machine. The speedup, on a per-simulation basis, is more than 2 000 000:1. This is the primary advantage of the ROM over the PDE model.

Fig. 1(a) shows room-temperature side-reaction current density J_s as computed by the reduced-order model (which we now denote as $J_{s,\text{ROM}}$). Fig. 1(b) shows a compilation of $J_{s,\text{ROM}}$ over a range of temperatures. We see two trends that match experience: degradation is worst at high SOC and high charge rates.

Fig. 2 shows results of one PDE simulation. This example was conducted at 25 °C, 50% SOC, and by applying a 1 C charge pulse at $t = 0.5$ s. The figure shows the raw output of the simulation, as compared to the ROM. Both the PDE and ROM solutions have a non-zero negative side reaction flux J_s even when the cell is at rest. This is due to the fact that we have relaxed Assumption 2 of the SEI growth model in Section 2 to also allow for the side reaction when current in the external circuit is zero. Fig. 2 shows that the ROM matches both the rest SEI side-reaction rate and the charge-pulse SEI side-reaction rate.

Plotted on the same scale, the full PDE solution results are indistinguishable from the ROM results. So, for comparison purposes, we define a relative error between the results as

$$J_{s,\text{err }\%} = \frac{J_{s,\text{PDE}} - J_{s,\text{ROM}}}{J_{s,\text{PDE}}} \times 100,$$

where $J_{s,\text{PDE}}$ is chosen to be the value of J_s from the PDE solution immediately after the application of the current pulse. Fig. 3 plots the relative error between the PDE and ROM solutions for all 25 °C simulations. Between 10% and 90% SOC, typical extremum operating conditions for electric vehicle battery cells, for example, the maximum relative error was 0.44%.

To further illustrate the performance of the ROM and to see the dependence of SEI layer growth rate on SOC and charge rate, Fig. 4 plots these results in a different format (25 °C). Frame (a) shows the side-reaction current density as a function of SOC at different charge rates (lines plotted from 0 C to 3 C in steps of 0.5 C), and

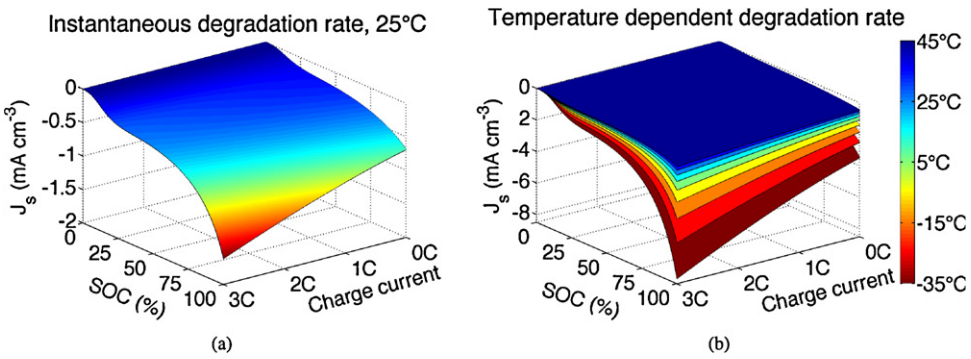

Fig. 1. Reduced-order model results for J_s: (a) at 25 °C; (b) at various temperatures.

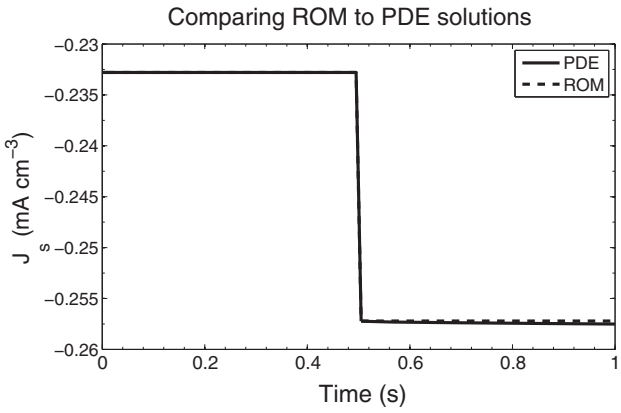

Fig. 2. An example PDE simulation result.

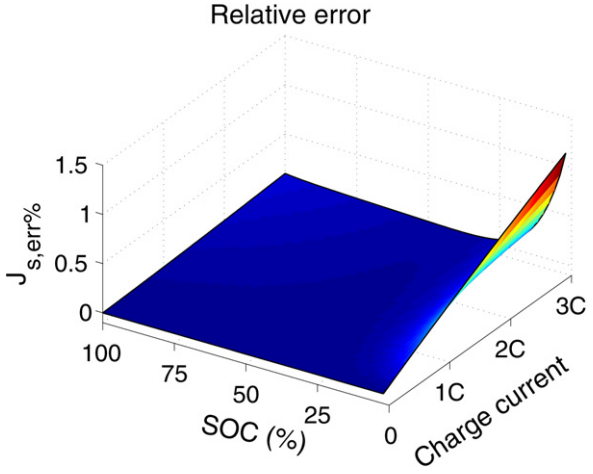

Fig. 3. Relative errors between PDE and ROM solutions.

Frame (b) shows the side-reaction current density as a function of charge rate at different SOCs (lines plotted from 0% SOC to 100% SOC in steps of 10% SOC). In all plots, the corrected PDE result is drawn as a solid line, and the ROM result is drawn as a dashed line. In most cases, it is impossible to visually distinguish between the PDE and ROM results.

Fig. 5 shows additional effects on relative error. Frame (a) shows how relative error varies with temperature. We see that the ROM predictions are best at high temperatures, and less good at low temperatures. Worst-case $J_{s,err\%}$ in the 10–90% SOC range varies from 0.41% at 45 °C to 0.55% at −35 °C. Frame (b) investigates the effect of Δt on the results. Instead of selecting the value for $J_{s,PDE}$ immediately after the application of the current pulse, $J_{s,PDE}$ is now selected to be the PDE solution 0.5 s after the application of the current pulse, at the $t = 1$ s point. We see from Fig. 2 that we expect a somewhat different result using this method; indeed, Fig. 5(b) verifies this observation. The relative error is once again worst at low temperatures and low values of SOC (where the absolute amount of degradation is small). Relative errors over 10% are observed in some cases, but in the ranges of SOC most important for control, where SOC is greater than 25%, the worst-case $J_{s,err\%}$ is far less, varying from 0.85% at 45 °C to 1.04% at −35 °C.

Fig. 6 investigates the effect of a prolonged constant-current charge at a 1 C rate, as might be experienced when a cell is being charged. The PDE is simulated for 3000 s, starting with the cell at rest at 10% SOC, and 1D profiles of $J_s(x)$ across the anode are plotted at time steps 100 s, 1000 s, 2000 s, and 3000 s. Overlaid on the plot are the average J_s values predicted by the ROM at that SOC level, and the actual averaged J_s values (averaged over the 1D electrode) from the PDE solution. In the ROM simulation, the SOC is updated on a second-by-second basis to achieve the present SOC at every point, which is used to compute the value of J_s using the method explained

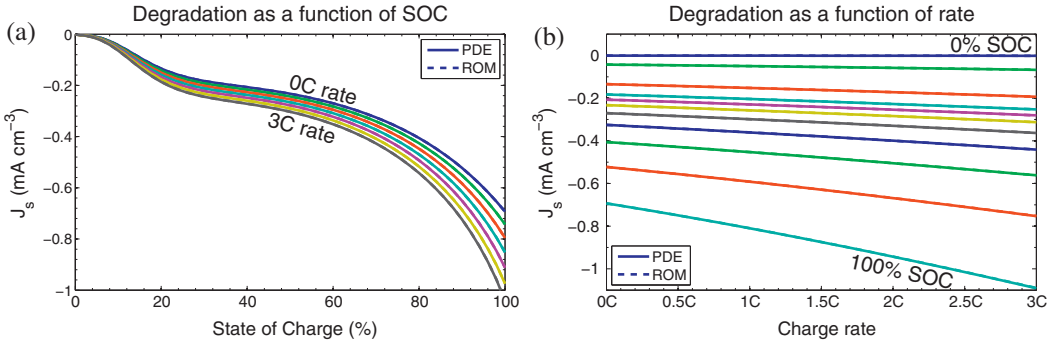

Fig. 4. Degradation as functions of SOC and rate.

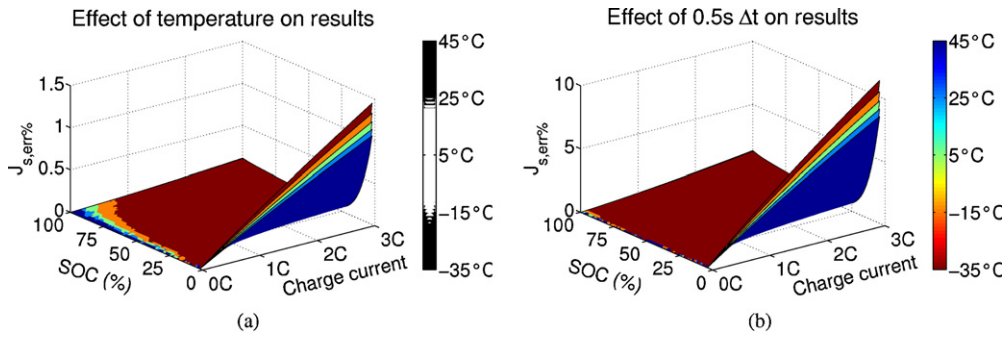

Fig. 5. Additional effects on relative error: (a) various temperatures; (b) a different Δt.

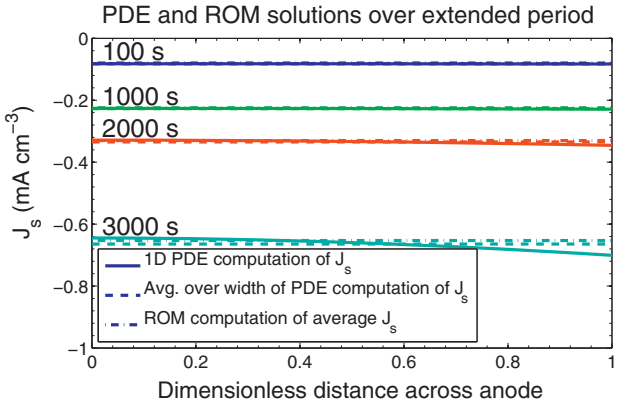

Fig. 6. Comparing PDE and ROM solutions over long 1 C charge.

in this paper. We see that even over prolonged constant-current charge profiles, the ROM is accurate, indicating that Assumption 1 of ROM (cf. Section 3) is a reasonable assumption to make.

5. Conclusion

From the results above, there is a clear advantage to having a reduced order model. The reduced order model takes the very difficult and time consuming procedure to calculate the governing equations necessary to obtain J_s in a PDE model, and reduces them to a very fast algebraic expression, Eq. (12), that a small microcontroller can easily calculate. As noted, the speedup is more than 2 000 000 : 1 when using the ROM *versus* the PDE solver. Further, from this simple calculation of J_s, an incremental model of degradation is obtained, Eqs. (13) and (14). The results themselves are very accurate, resulting in about 0.5% relative error at the instant of applied current to about 1% relative error 0.5 s later, for SOC ranges of interest.

Due to the high-fidelity approximation of J_s, we expect that control actions taken using $J_{s,\mathrm{ROM}}$ will closely approximate those taken using $J_{s,\mathrm{PDE}}$. Therefore, this model shows potential for being used in an optimal charger design. This would allow a battery to be charged very quickly, but also allow the microcontroller to optimize the charging profile easily in order to avoid unnecessary degradation. In a future paper, the authors will explain their current research into optimal profiles that consider SEI growth as well as other degradation mechanisms.

Acknowledgments

Financial support for the research reported in this paper has been received from the General Motors/University of Michigan Advanced Battery Coalition for Drivetrains (GM/UM ABCD), to which the University of Colorado Colorado Springs is a subcontractor. Mr. Randall would also like to thank his wife for being patient, kind, and loving during his research, and the Lord for giving him all of his abilities to do research.

Appendix A. Model equations

The following is a summary of the governing equations for the model developed in [4] and used in [9] for ideal cell dynamics. The conservation of lithium in a single particle is modeled by Fick's law of diffusion

$$\frac{\partial c_s}{\partial t} = \frac{D_s}{r^2}\frac{\partial}{\partial r}\left(r^2\frac{\partial c_s}{\partial r}\right),$$

with boundary conditions

$$\left.\frac{\partial c_s}{\partial r}\right|_{r=0} = 0 \quad \text{and} \quad D_s\left.\frac{\partial c_s}{\partial r}\right|_{r=R} = \frac{-J_I}{a_s F},$$

where c_s is the solid-phase lithium concentration (the subscript s denotes the solid phase), D_s is the solid phase diffusion coefficient, J_I is the volumetric rate of electrochemical reaction at the particle surface, a_s is the specific interfacial surface area, and F is Faraday's constant. For a spherical particle of active material that has a radius R in an electrode with volume fraction of active material ε_s, the interfacial surface area is $a_s = 3\varepsilon_s/R$.

Conservation of lithium in the electrolyte phase gives the following equation:

$$\frac{\partial(\varepsilon_e c_e)}{\partial t} = \frac{\partial}{\partial x}\left(D_e^{\mathrm{eff}}\frac{\partial}{\partial x}c_e\right) + \frac{1-t_+^0}{F}J_I,$$

which has the following zero flux boundary conditions at the current collectors,

$$\left.\frac{\partial c_e}{\partial x}\right|_{x=0} = \left.\frac{\partial c_e}{\partial x}\right|_{x=L} = 0,$$

where c_e is the electrolyte phase lithium concentration (the subscript e denotes the electrolyte phase), ε_e is the electrolyte phase volume fraction and t_+^0 is the transference number of Li^+ with respect to the solvent velocity, which is assumed constant. The effective diffusion coefficient is calculated from a reference coefficient using the Bruggeman constant, $D_e^{\mathrm{eff}} = D_e\varepsilon_e^{\mathrm{brug}}$. The Bruggeman relation takes into account the tortuosity of the path the Li^+ ions take through the electrode.

Charge conservation in the solid phase in the electrodes is described by Ohm's law,

$$\frac{\partial}{\partial x}\left(\sigma^{\mathrm{eff}}\frac{\partial}{\partial x}\phi_s\right) - J_I = 0,$$

with boundary conditions at the current collector,

$$-\sigma^{\text{eff}}\left.\frac{\partial\phi_s}{\partial x}\right|_{x=0} = \sigma^{\text{eff}}\left.\frac{\partial\phi_s}{\partial x}\right|_{x=L} = \frac{I}{A} = i_{\text{app}},$$

where ϕ_s is the potential of the solid, $\sigma^{\text{eff}} = \sigma\varepsilon_s^{\text{brug}}$ is the effective conductivity of the solid, A is the electrode plate area, and I is the applied current, where a positive current discharges the battery. There must be zero electronic current at the separator boundary, so

$$\left.\frac{\partial\phi_s}{\partial x}\right|_{x=L_{n,\text{sep}}} = \left.\frac{\partial\phi_s}{\partial x}\right|_{x=L_{p,\text{sep}}} = 0.$$

Conservation of charge in the electrolyte gives the equation

$$\frac{\partial}{\partial x}\left(\kappa^{\text{eff}}\frac{\partial}{\partial x}\phi_e\right) + \frac{\partial}{\partial x}\left(\kappa_D^{\text{eff}}\frac{\partial}{\partial x}\ln(c_e)\right) + J_I = 0,$$

where ϕ_e is the potential of the electrolyte phase, and κ^{eff} is the effective ionic conductivity, calculated from the Bruggeman relation,

$$\kappa^{\text{eff}} = \kappa\varepsilon_e^{\text{brug}} = (4.1253\times10^{-4} + 5.007c_e - 4.7212\times10^{3}c_e^2 + 1.5094\times10^{6}c_e^3 - 1.6018\times10^{8}c_e^4)\varepsilon_e^{\text{brug}}$$

$$\kappa_D^{\text{eff}} = \frac{2R_gT\kappa^{\text{eff}}}{F}\left(t_+^0 - 1\right)\left(1 + \frac{\mathrm{d}\ln(f_\pm)}{\mathrm{d}\ln(c_e)}\right),$$

where R_g is the universal gas constant, T is the temperature and $f_\pm$ is the activity coefficient, assumed here to be constant (its derivative is zero). This equation has boundary conditions

$$\left.\frac{\partial\phi_e}{\partial x}\right|_{x=0} = \left.\frac{\partial\phi_e}{\partial x}\right|_{x=L} = 0.$$

The PDEs are coupled via the intercalation current density

$$J_I = a_j i_{0,j}\left[\exp\left(\frac{\alpha_{a,j}F}{R_gT}\eta_j\right) - \exp\left(-\frac{\alpha_{c,j}F}{R_gT}\eta_j\right)\right], \qquad j = n, p$$

which is driven by the overpotential

$$\eta_j = \phi_s - \phi_e - U_j^{\text{ref}} - \frac{J_{\text{total}}}{a_j}R_{\text{film}},$$

where i_0 is the exchange current density,

$$i_{0,j} = k_j\left(c_{s,j}^{\max} - c_{s,j}\right)^{\alpha_{a,j}}\left(c_{s,j}\right)^{\alpha_{c,j}}(c_e)^{\alpha_{a,j}}, \qquad j = n, p$$

and U_j^{ref} is the equilibrium potential which is evaluated as a function of the solid phase concentration at the surface of the particle. For this work,

$$U_n^{\text{ref}} = 0.7222 + 0.1387\theta_n + 0.029\theta_n^{1/2} - \frac{0.0172}{\theta_n} + \frac{0.0019}{\theta_n^{1.5}} + 0.2808\exp\left(0.90 - 15\theta_n\right) - 0.7984\exp\left(0.4465\theta_n - 0.4108\right) \quad (15)$$

$$U_p^{\text{ref}} = \frac{(-4.656 + 88.669\theta_p^4 + 342.909\theta_p^4 + 342.909\theta_p^6 - 462.471\theta_p^8 + 433.434\theta_p^{10})}{(-1 + 18.933\theta_p^2 - 79.532\theta_p^4 + 37.311\theta_p^6 - 73.083\theta_p^8 + 95.96\theta_p^{10})}.$$

References

[1] M. Broussely, P. Biensan, F. Bonhomme, P. Blanchard, S. Herreyre, K. Nechev, R. Staniewicz, Journal of Power Sources 146 (2005) 90–96.
[2] M. Broussely, S. Herreyre, P. Biensan, P. Kasztejna, K. Nechev, R. Staniewicz, Journal of Power Sources 97–98 (2001) 13–21.
[3] R. Darling, J. Newman, Journal of the Electrochemical Society 145 (1998) 990–998.
[4] M. Doyle, T.F. Fuller, J. Newman, Journal of the Electrochemical Society 140 (1993) 1526–1533.
[5] T.F. Fuller, M. Doyle, J. Newman, Journal of the Electrochemical Society 141 (1994) 1–10.
[6] M.D. Levi, G. Salitra, B. Markovsky, H. Teller, D. Aurbach, U. Heider, L. Heider, Journal of the Electrochemical Society 146 (1999) 1279–1289.
[7] M.D. Levi, D. Aurbach, Journal of Electroanalytical Chemistry 421 (1997) 79–88.
[8] J. Vetter, P. Novák, M. Wagner, C. Veit, K.-C. Möller, J. Besenhard, M. Winter, M. Wohlfahrt-Mehrens, C. Vogler, A. Hammouche, Journal of Power Sources 147 (2005) 269–281.
[9] P. Ramadass, B. Haran, P.M. Gomadam, R. White, B.N. Popov, Journal of the Electrochemical Society 151 (2004) A196–A203.
[10] S. Moura, J. Forman, S. Bashash, J. Stein, H. Fathy, IEEE Transactions on Industrial Electronics 58 (2011) 3555–3566.
[11] N.A. Chaturvedi, R. Klein, J. Christensen, J. Ahmed, A. Kojic, IEEE Control Systems Magazine 30 (2010) 49–68.
[12] K.A. Smith, C.D. Rahn, C.-Y. Wang, Energy Conversion and Management 48 (2007) 2565–2578.
[13] R. Spotnitz, Journal of Power Sources 113 (2003) 72–80.
[14] D. Aurbach, B. Markovsky, I. Weissman, E. Levi, Y. Ein-Eli, Electrochimica Acta 45 (1999) 67–86.
[15] A.V. Churikov, Electrochimica Acta 46 (2001) 2415–2426.
[16] I. Nainville, A. Lemarchand, J.P. Badiali, Electrochimica Acta 41 (1996) 2855–2863.
[17] O. Pensado-Rodriguez, J.R. Flores, M. Urquidi-Macdonald, D.D. Macdonald, Journal of the Electrochemical Society 146 (1999) 1326–1335.
[18] COMSOL Multiphysics, online: http://www.comsol.com/ (accessed 24.10.11).
[19] MATLAB-x, online: http://www.mathworks.com/ (accessed 24.10.11).
[20] P. Ramadass, Capacity Fade Analysis of Commercial Li-Ion Batteries, Ph.D. Thesis, University of South Carolina, 2003.